Articles in PresS. J Neurophysiol (June 16, 2010). doi:10.1152/jn.00178.2010

Inhibitory modulation of cortical up states

Maria V. Sanchez-Vives,[1,2]* Mauzio Mattia,[3] Albert Compte,[1] Maria Perez-Zabalza,[1] Milena Winograd,[4] Vanessa F. Descalzo,[1] and Ramon Reig [1]

[1] IDIBAPS (Institut d'Investigacions Biomèdiques August Pi i Sunyer), Barcelona, Spain
[2] ICREA (Institució Catalana de Recerca i Estudis Avançats), Barcelona, Spain
[3] Istituto Superiore di Sanità, Roma, Italy
[4] Instituto de Neurociencias de Alicante, UMH-CSIC, 03550 San Juan de Alicante, Spain

Running title: Inhibition and cortical up states

Contact information:
Maria V. Sanchez-Vives
IDIBAPS
Villarroel, 170
08036 Barcelona
Tel (34) 93 2275400 ext 4301
e-mail: msanche3@clinic.ub.es; sanchez.vives@gmail.com

Abstract

The balance between excitation and inhibition is critical in the physiology of the cerebral cortex. To understand the influence of inhibitory control on the emergent activity of the cortical network, inhibition was progressively blocked in a slice preparation that generates spontaneous rhythmic up states at a similar frequency to those occurring *in vivo* during slow wave sleep or anesthesia. Progressive removal of inhibition induced a parametric shortening of up state duration and elongation of the down states, the frequency of oscillations decaying. Concurrently, a gradual increase in the network firing rate during up states occurred. The slope of transitions between up and down states was quantified for different levels of inhibition. The slope of upward transitions reflects the recruitment of the local network and was progressively increased when inhibition was decreased, while the speed of activity propagation became faster. Removal of inhibition resulted eventually in epileptiform activity. While gradual reduction of inhibition induced linear changes in up/down states and their propagation, epileptiform activity was the result of a nonlinear transformation. A computational network model showed that strong recurrence plus activity-dependent hyperpolarizing currents were sufficient to account for the observed up state modulations and predicted an increase in activity-dependent hyperpolarization following up states when inhibition was decreased which was confirmed experimentally.

Keywords: Cerebral Cortex / In vitro / Epilepsy / GABAergic / Slow oscillations

Introduction

The issue of how excitation and inhibition are regulated in the course of physiological network function is highly relevant to understand cortical physiology and its dysfunctions, as for instance in epilepsy. A model where the engagement of excitation and inhibition in cortical function can be studied is slow oscillatory activity. Basal excitability and recurrent connectivity in the cerebral cortex (Hebb 1949; Lorente de Nó 1938) induces neuronal firing that reverberates in the circuit, resulting in the emergent network activity. During slow-wave sleep and anesthesia, this activity is organized in the cerebral cortex in a slow (<1Hz) rhythmic pattern consisting of interspersed up and down states (Lampl et al. 1999; Steriade et al. 1993; Stern et al. 1997). This activity can also be generated in cortical slices maintained *in vitro* (Sanchez-Vives and McCormick 2000), therefore providing a range of experimental models, from *in vitro* to sleeping animals.

Several lines of evidence confirm that both excitatory and inhibitory neurons participate in the firing during up states. The first study that presented a detailed description of slow oscillations (Steriade et al. 1993) reported that not only excitatory electrophysiological types but also inhibitory ones (fast spiking neurons) fired during up states, extent that was confirmed by subsequent studies (Contreras et al. 1996; Cowan and Wilson 1994; Sanchez-Vives and McCormick 2000; Steriade et al. 1993; Steriade et al. 2001). Furthermore, both excitatory and inhibitory synaptic potentials coexist during up states both *in vivo* and *in vitro*, and the relative contribution of excitation and inhibition to cortical activity has been estimated mainly through conductance changes (Anderson et al. 2000; Borg-Graham et al. 1998; Haider et al. 2006; Okun and Lampl 2008; Pare et al. 1998; Rudolph et al. 2007; Shu et al. 2003b) or through the timing of excitatory and inhibitory events (Compte et al. 2008; Compte et al. 2009).

The general understanding achieved by different methods is that excitation and inhibition balance each other, and this has been reported both during spontaneous and sensory activated cortical activity (Anderson et al. 2000; Haider et al. 2006; Monier et al. 2008; Okun and Lampl 2008; Shadlen and Newsome 1998; Shu et al. 2003b; Wehr

and Zador 2003). Imbalance of excitation and inhibition in cortex and hippocampus is not only related to epilepsy (Brown et al. 1996; Gutnick et al. 1982; Kumar and Buckmaster 2006) but has been as well associated to mental retardation syndromes such as Rett disorder (Dani et al. 2005), Down Syndrome (Belichenko et al. 2004; Fernandez et al. 2007; Hanson et al. 2007; Kurt et al. 2004), or autism (Rubenstein and Merzenich 2003), making the understanding of the physiological excitatory/inhibitory balance highly relevant.

What we explore here is how the network activity and its propagation are modified when inhibition is progressively blocked, and which are the possible involved mechanisms in a computational cortical model, finally testing its predictions experimentally.

Materials and Methods

Ferrets (2-12 month old, either sex) were anesthetized with sodium pentobarbital (40 mg/kg) and decapitated. The entire forebrain was rapidly removed to oxigenated cold (4-10^{o}C) bathing medium. Coronal slices (0.4 mm thick) from the occipital cortex containing primary and secondary visual cortical areas (areas 17, 18, and 19) (Innocenti et al. 2002) or prefrontal (Krimer and Goldman-Rakic 2001) were used.

A modification of the sucrose-substitution technique developed by (Aghajanian and Rasmussen 1989) was used to increase tissue viability. During preparation of slices, the tissue was placed in a solution in which NaCl was replaced with sucrose while maintaining an osmolarity of 307 mOsm. After preparation, slices were placed in an interface style recording chamber (Fine Sciences Tools, Foster City, CA). For the first 15 minutes cortical slices were superfused with an equal mixture in volume of the normal bathing medium and the sucrose-substituted solution. Following this, normal bathing medium was switched into the chamber and superfused the slices for 1-2 hours, then modified slice solution was used throughout the rest of the experiment. Bath temperature was maintained at 34.5-36^{0} C.

The normal bathing medium contained (in mM): NaCl, 126; KCl, 2.5; $MgSO_4$, 2; NaH_2PO_4, 1.25; $CaCl_2$, 22; $NaHCO_3$, 26; dextrose, 10, and was aerated with 95% O_2, 5% CO_2 to a final pH of 7.4. The modified solution had the same ionic composition except for different levels of (in mM) KCl, 3.5; $MgSO_4$, 1 and $CaCl_2$, 1-1.2 (Sanchez-Vives and McCormick 2000). Electrophysiological recordings started after allowing at least 2 hours recovery.

Drugs were applied either in the bath or locally, through the delivery of a brief pressure pulse (10-150 ms; 100-350 KPa) to a drug-contanining micropipette (volumes of 1-20 pl per pulse). Drugs used were bicuculline methiodide, SR95531 (gabazine) both of them from Sigma

Spike recording and analysis

Extracellular multiunit recordings were obtained with 2-4 MΩ tungsten electrodes (FHC, Bowdoinham, ME).

Multiunit activity (MUA) was estimated as the power change in the Fourier components at high frequencies of the recorded local field potentials (LFP) (Reig et al. 2010). High frequency components of LFP can be seen as a linear transform of the instantaneous firing rate of the neurons surrounding the electrode tip. We assume then that the normalized LFP spectra provides a good estimate of the population firing rate, given that Fourier components at high frequencies have densities proportional to the spiking activity of the involved neurons (Mattia and Del Giudice 2002). The time-dependent MUAs were the average power of the normalized spectra in the frequency band (0.2-1.5) kHz. With respect to a similar approach in (Stark and Abeles 2007), the above estimate provides a larger signal-to-noise ratio: using normalized spectra the components at different frequencies have similar orders of magnitude. MUAs were logarithmically scaled to balance the large fluctuations of the nearby spikes. Furthermore, log(MUA) time series were smoothed by a moving average with a sliding window of 80 ms.

Up and down states were singled out by setting a threshold in log(MUA) time series. The histograms of log(MUA) were bimodal and the positions of the high and low peaks were used as reference activity respectively for up and down states. The discriminating threshold was set to the 60% of the interval between the peaks. To remove the effects of small activity fluctuations a cut-off in the minimum state duration was set in a range $[1/3,\ 1/2]$ of the average up state length. This lower limit was chosen case-by-case in order to reproduce the up/down oscillation frequency estimated from the log(MUA) autocorrelation. Small periods were recursively removed converting short up (down) states in longer down (up) states. Finally, times of transition between states were better estimated by fitting the log(MUA) in a 100 ms window around the transitions with third degree polynomials. The adjusted transition was set to the crossing time of the polynomial with the discriminating threshold. These polynomials were furthermore used to estimate the slope of transitions given by the gradient around the previously detected crossing times. The slopes of the upward transitions were measured as the

gradients of the linear fits of the average log(MUA) in the time interval (-10, 25 ms) around the detected up state onset. Similarly, the slopes of the downward transitions resulted from the linear fit of log(MUA) centered around the occurrences of the transitions to down states in the time interval (-25, 10 ms).

All the MUA off-line estimates and analyses were implemented in MATLAB (The MathWorks Inc., Natick, MA). We refer to the log(MUA) spectra in the figures and the rest of the manuscript as "relative firing rate", since is a relative measure resulting from an average of power spectra ratios (Reig et al. 2010).

Intracellular recordings

Sharp intracellular recording electrodes were formed on a Sutter Instruments (Novato, CA) P-97 micropipette puller from medium-walled glass (1B100F-4, WPI Sarasota, FL) and beveled on a Sutter Instruments beveller to final resistances of 60-100 MOhms. Micropipettes were filled with 2 M KAc. Current clamp intracellular recordings were obtained using an Axoclamp 2B amplifier (Axon Instruments, Foster City, CA). The transitions between up and down states in the intracellular recordings illustrated below were detected by hand in order to determine their slopes. Intra and extracellular recordings were digitized, acquired and analyzed with a CED interface and Spike 2 software (Cambridge Electronic Design, Cambridge, UK). Data are reported as mean ± SD.

Computational modelling

We use the network model of slow oscillatory activity in visual cortical slices of the ferret that has been presented elsewhere (Compte et al. 2003). Briefly, the network model consists of a population of 1024 pyramidal cells and 256 inhibitory interneurons equidistantly distributed on a line and interconnected through biologically plausible synaptic dynamics (kinetics of synaptic currents mediated by AMPARs, NMDARs, and $GABA_A$Rs are modeled as in (Wang 1999). Some of the intrinsic parameters of the cells are randomly distributed, so that the populations are heterogeneous. This, and the random connectivity (determined by the synaptic probability distributions; see Figure

7A) are the only sources of noise in the network. The neurons in the network are sparsely connected to each other through a fixed number of connections that are set at the beginning of the simulation. Neurons make 20 ± 5 contacts (mean ± standard deviation) with their postsynaptic partners (multiple contacts onto the same target, but no autapses are allowed). For each pair of neurons separated by a distance x in the network, the probability that they are connected in each direction is decided by a Gaussian probability distribution $P(x)$ centered at 0 and with a prescribed standard deviation σ_E. For inhibitory connections a Gaussian probability distribution is also used but with a smaller standard deviation $\sigma_I=\sigma_E/2$. Our model pyramidal cells have a somatic and a dendritic compartment. The somatic compartment hosts the spiking currents, I_{Na} and I_K, a leak current I_L, a fast A-type K^+-current I_A, a non-inactivating slow K^+-current I_{KS} and a Na^+-dependent K^+-current I_{KNa}. The dendrite contains a highthreshold Ca^{2+} current I_{Ca}, a Ca^{2+}-dependent K^+-current I_{KCa}, a non-inactivating (persistent) Na^+ current I_{NaP} and an inward rectifier (activated by hyperpolarization) non-inactivating K^+ current I_{AR}. For interneurons the model was taken from (Wang and Buzsaki 1996). All details about the exact parameter values and model implementations can be found in (Compte et al. 2003). The model was implemented in a C++ code and simulated using a fourth-order Runge-Kutta method with a time-step of 0.06 ms.

Results

Fifty-five slices of ferret visual or prefrontal cortex that generated spontaneous slow rhythmic activity were recorded (<1 Hz; Fig. 1). Spontaneous rhythmic activity consisted on alternating periods of persistent activation or *up states* interleaved with intervals of relative silence or *down states*. In order to understand how inhibition shapes emergent cortical activity, we acted on fast inhibition by decreasing it with bicuculline or gabazine. The removal of inhibition is known to result in epileptiform activity (Gutnick et al. 1982; Prince and Wilder 1967). Our main objective was to explore how the progressive blockade of $GABA_A$ receptors would transform cortical rhythmicity before the network became epileptic.

Effect of decreasing inhibition on the frequency and duration of up states

To explore how inhibition controls emerging network activity we applied a low concentration of BMI (bicuculline methiodide) in the bath (0.1-0.2 μM) and increased progressively the concentration until epileptiform activity would appear (usually >1 μM). Once full-blown epileptiform activity was generated (see below), further increase in BMI was not followed by any more gradual changes.

The progressive blockade of inhibition induced different concurrent changes in the physiological up and down states. Some of them are illustrated in Figure 1 for a particular slice. A progressive removal of inhibition induced a gradual shortening of up states. This can be observed in the raw traces in Fig. 1A, in raster plots in Fig. 1B, and in up state averages for seven BMI concentrations in Fig. 1C and 1F. The shortening of up states was concomitant with a progressive increase in the firing rate (Fig. 1C,E,G). The duration of the subsequent down states was also modified, becoming progressively longer with lesser inhibition (Fig. 1A-D). This example illustrates that there is a global change in the dynamics of the network activation as a result of inhibition removal. On the other hand, the bistable nature of the network activity remains unchanged and even at higher BMI concentrations two preferred activity levels can be recognized (Fig. 1E).

For a detailed quantification of activity transformation during gradual blockade of inhibition only slow oscillations of >0.2 Hz frequency were included (n=25), in order to

have up/down state dynamics similar to those *in vivo*. The transformation of the emergent activity described above (Fig. 1) following the removal of inhibition was consistent across the population: decrease in the up/down cycle frequency (Fig. 2A), increase in the firing rate during up states (Fig. 2B), shortening of up states (Fig. 2C), lengthening of down states (Fig. 2D). Similar results concerning isolated up states have been described (Mann et al. 2009).

Since bicuculline is known to have an additional effect to inhibition blockade which is the blockade of small K^+ channels (Debarbieux et al. 1998; Khawaled et al. 1999), we also used gabazine (SR95531) (n=11), a blocker of inhibition that does not have such collateral effect. The specific effects of SF95531 on the spontaneous activity are represented in supplemental Fig. S1, illustrating that the network effects were equivalent to those obtained for bicuculline: the frequency of the oscillation decreased , the firing rate during up states increased, up state duration decreased and down state duration increased. Even when there were no statistically significant differences with bicuculline-induced changes (except for the slope of down states increase), we observed that in gabazine both the increase in up state's firing rate and the elongation of down states were lesser than in BMI.

Removal of inhibition and the upward and downward network transitions

We measured the slopes of the network transition from down to up states (Fig. 3A). The upward transition reflects the recruitment of the local network. Increasing concentrations of BMI (Fig. 3A) or gabazine (supplemental Fig. S1) resulted in a progressively faster recruitment of the local network, and thus a faster upward transition. This was the case at the population level (Fig. 3B). The slope measured at the initiation of epileptiform discharges revealed a still faster recruitment, usually doubling the one reached in the pre-epileptic state (Fig. 3B). The local network recruitment has its cellular counterpart in the summation of synaptic potentials impinging onto a particular neuron. Eleven intracellular recordings were included: 9 regular spiking, 1 chattering cell and 1 intrinsically bursty neuron, classification done following (Nowak et al. 2003). Intracellular recordings (Fig. 3E) illustrate the

accumulation of synaptic events that leads to an up state, accumulation that becomes faster with the progressive removal of inhibition. This faster transition can be observed also in the transformation from slow wave activity to epileptiform activity *in vivo* (Steriade and Contreras 1995). These results suggest that in physiological conditions inhibition is slowing down the recruitment of activity in the local network. The slower/faster recruitment of the local network also results in the control of the propagation of activity (Compte et al. 2003) (see below).

The downward transition from up to down states marks the end of up states. The slope of this transition was as well evaluated at the network level by measuring the decay in the local relative firing rate (Fig. 3C). The progressive removal of inhibition also lead to a steeper downward transition, reflecting that the transition is occurring more synchronously in the local population. This was also the case when all slices were considered (Fig. 3D). In the case of the downward transition, epileptiform responses did not have a faster downward transition but a slower one. In conclusion, there was a parametric linear relation between removal of inhibition and increase in upward (downward) slope, and in both cases this relation became nonlinear when epileptiform activity appeared. The intracellular correlate of the increased downward transition is a faster repolarization of the up states while they became shorter (Fig. 3E). We provide a possible mechanistic explanation below, based on observations in a computational model.

In the course of gradual blockade of inhibition we often (56%) observed what we refered to as “diplets” or even “triplets” (Fig. 4). Diplets (triplets) where up states of shorter duration and higher firing frequency that appeared in pairs (trios) (Fig. 4B, C, F), as if they were up states fractioned into two (three) parts. This activity was most often transitory, suggesting a short-lived activity occurring while the network was adapting to a lower level of inhibition (Fig. 4E). No relationship was found between the occurrence of diplets and the generation of epileptiform discharges. Even when this may be a phenomenon of inherent interest, in order to quantify the evolution of up states with changing inhibition as in Fig.2, diplets (triplets) were excluded.

Inhibition and the wave propagation speed

The speed of propagation of the wave reflects the horizontal propagation of the locally generated up states along the cerebral cortex. By horizontal we refer to the propagation perpendicular to the cortical columns and along cortical layers. We know that the speed of the travelling wave increases around one order of magnitude when inhibition is removed completely (Compte et al. 2003; Sanchez-Vives and McCormick 2000). Here we found that the speed of wave propagation increased linearly with the progressive removal of inhibition. Up states were recorded with two separate electrodes (Fig. 5A) and the time lags between the initiation of every up state recorded from both electrodes were measured for different bicuculline concentrations (Fig. 5B). The distribution of time lags for each bicuculline concentration was calculated, and the mean time that the activity takes to travel from one electrode to the other was taken as the peak. Sometimes the activity would travel in the opposite direction and then bimodal histograms of time lags occur with almost symmetrical peaks: in these cases we considered the most populated peak to estimate the speed of propagation.

The average speed of propagation determined in that way was calculated in 5 slices for 5 concentrations of BMI (Fig. 5C). Before reaching epileptiform activity, the speed of propagation of activity had approximately doubled (from 6 to 12 mm/s). However the increase in speed once full-blown epileptiform activity occurred was nonlinear with the previous ones, reaching an average speed of 43 mm/s. During activity propagation, up states are locally regenerated along the network, such that the initiation of up states appears intracellularly as a summation of synaptic potentials (Fig. 3E). The local recruitment of network activity is also represented by the transition from down to up states of the firing rate (Fig. 3A, B). We observed that the faster the down to up state transition is, the faster the speed of wave propagation (Fig. 5D), thus the local build up of the upward transition influences the speed of the wave.

Transition towards epileptiform discharges

We further investigated the changes at higher levels of disinhibition capable to elicit the onset of epileptic-like activity. Full-blown epileptiform discharges occurred

unexpectedly as a dramatic and sustained increase of activity simultaneously observable from distant electrodes as in Fig. 6A (at ca. 460 ms). Dynamics of probed populations of neurons had an abrupt and qualitative change as witnessed by the time course of the latency between the onset of up states detected by distant electrodes (Fig. 6A, bottom panel), showing a discontinuity in the speed of propagation that induced an almost simultaneous state transition in different points of the slice (see also Fig. 5C).

When inhibition is progressively removed, there is a transformation of the emergent pattern of activity until eventually becomes epileptiform. This transformation is illustrated in Fig. 6D. Stage 0 represents up states and down states during physiological slow oscillations. As we have characterized in this study, up states become progressively shorter with inhibition blockade, and this is illustrated in Stage 1: shorter up states and elongated down states. The parametric changes in up/down states induced by a progressive removal of inhibition described above correspond to the transformation between Stage 0 and Stage 1 (Figs. 1, 2). Before full-blown epileptiform discharges appear (Stage 3), there are short bursts of activity of steep rise characterized by their triangular or cuneiform shape (Stage 2), instead of the fusiform shape of up states in Stages 0 and 1. The triangular (or cuneiform) shape corresponds to an abnormally fast recruitment of the local network, inducing a heavy spike discharge and that has a progressive decay. This pattern of activity may be local (Fig. 6B) or propagate between electrodes.

Computational modelling and predictions

In order to test the consistence of our findings with our mechanistic interpretation, we used a previously defined computational network model of the slow oscillation (Compte et al., 2003), which relies on strong recurrent coupling and activity-dependent potassium channels for the generation of the slow rhythm. This model consists of 1,024 excitatory cells and 256 inhibitory cells modeled with detailed Hodgkin-Huxley-type channels and interconnected through realistic synaptic dynamics (Materials and Methods). Critical for the model behavior is strong recurrent excitation and inhibition, and Ca^{2+}- and Na^{+}-dependent potassium channels in pyramidal cells,

368 which are responsible for the transitions between up and down states. The model
369 network displays activity organized in recurring up states that propagate across the
370 network, closely resembling the experimental data (Compte et al., 2003; Compte et al.,
371 2008; Compte et al., 2009).

372 We wanted to study what effects progressive inhibition blockade induced in the
373 network activity of the computer model in (Compte et al., 2003). Because we know in
374 detail the mechanisms that generate the network activity in the model (Compte et al.,
375 2003), this tested specifically our mechanistic understanding of the experimental
376 results. The removal of inhibition was simulated by the reduction of $GABA_A$ channel
377 conductances in inhibitory synapses to pyramidal neurons of the network. This
378 manipulation resulted in increased excitability, as measured by the firing rate of
379 neurons during the up state (Fig. 7C), but also induced significant reductions in the
380 duration of the up states (Fig. 7D,E) and an increase in the interval between oscillations
381 (Fig. 7C, E), in agreement with the experimental results. In addition, the model also
382 reproduced the augmented slope of down-to-up activity build-up after inhibition
383 blockade (Fig. 7D) and the progressive increase in wave propagation speed as inhibition
384 was gradually blocked (Fig. 10B in Compte et al., 2003). We explored what model
385 mechanisms were underpinning these network activity changes. The membrane
386 potential traces of excitatory neurons in the network revealed a larger
387 afterhyperpolarization (AHP) following up states after inhibition was decreased (Fig.
388 7F). This observation led us to suggest that the activation of K^+ channels with the
389 neuronal firing during up states could be a relevant mechanism in the termination of
390 up states (Compte et al. 2003; Cunningham et al. 2006), some of which could be
391 associated to $GABA_B$ receptors (Mann et al. 2009; Parga and Abbott 2007). The
392 outcome of our investigations of the computational network model therefore prove that
393 the combination of strong recurrent feedback and activity-dependent potassium
394 currents is sufficient to explain the typical modulations of network activity patterns
395 observed upon inhibition manipulation.

396

397

Experimental testing of model predictions

Intracellular recordings from neurons in a network with reduced inhibition revealed that AHPs following up states showed increased amplitude relative to control conditions with intact inhibition (Fig. 8), as predicted by the model (Fig. 7F). An increase in the afterhyperpolarization following up states with the removal of inhibition is suggestive of a more efficiently recruited mechanism to terminate up states. This is compatible with the increased firing rate during up states with lesser inhibition (Fig. 1, 2). Consistent with this, the increase in firing rate during up states was significantly correlated with the slope of the subsequent downward transition (Fig. Supplemental Fig. S2).

Discussion

We studied the functional contribution of inhibition to the slow oscillatory patterns generated by the cortical network *in vitro*. It is agreed that excitation and inhibition balance each other both during spontaneous and sensory activated cortical activity (Anderson et al. 2000; Compte et al. 2009; Haider et al. 2006; Monier et al. 2008; Okun and Lampl 2008; Shadlen and Newsome 1998; Shu et al. 2003a; Wehr and Zador 2003). When this balance is altered, pathological patterns of activity such as epilepsy are generated (Prince and Wilder 1967; Steriade et al. 1998; Timofeev et al. 2002). Our objective was to analyze from a network perspective how inhibition regulates cortical emergent activity by inducing a progressive excitatory/inhibitory imbalance.

Progressive reduction of inhibition resulted in a parametric decrease in the duration and frequency of up states. As a result, lesser inhibition lead to an apparently decreased activity in the network (see Fig. 1B), a rather counterintuitive effect. We suggest here that the link between reduction of inhibition and shorter and less frequent up states is the concurrent, parametric increase in firing rate during up states. Our investigations with a computational model of the slow oscillation (Compte et al., 2003) show that activity-dependent K^+ channels together with strong intracortical recurrence are sufficient to account for our typical experimental results (Fig. 7). In this reduced model of a cortical network, lesser inhibition during up states leads to higher firing rates, that recruit more efficiently activity-dependent K^+ channels, shortening up states and elongating down states. In support of the proposed mechanism there are various experimental results showing, on one hand that the higher the firing rate during up states, the longer down states become (Fig. 2B,D). On the other hand, the firing rate during up states was significantly correlated with the up to down state slope that reflects how fast network activity decreases at the end of up states (Supplemental Fig. 2. Thus, the larger the firing rate during the up state, the faster the silencing of the network. Furthermore, the increased AHP following up states when there is lesser inhibition also supports this mechanism (Fig. 8). Potassium channels are plausible candidates to initiate and maintain down states (Compte et al. 2003; Cunningham et al.

2006; Sanchez-Vives and McCormick 2000) and the main results presented here concur with this working model, although other activity-dependent mechanisms such as synaptic depression (Holcman and Tsodyks 2006) or $GABA_B$ activation (Mann et al. 2009; Parga and Abbott 2007) may also participate.

These results suggest that the transformation of the emergent activity when inhibition is decreased requires a dynamic interplay between up and down states. For that to occur is necessary that the oscillatory frequency is close to the physiological one. The frequency of slow oscillations was originally described as being <1Hz (Steriade et al. 1993), specifically 0.3-0.4 Hz in association (areas 5 and 7), motor and visual cortical areas of the anesthetized cat. The same frequency (0.3 Hz) was described in the ferret visual and prefrontal cortex *in vitro* and cat visual cortex *in vivo* (Sanchez-Vives and McCormick 2000). Rat neocortex *in vivo* generates higher frequencies, in the range 0.3-1.5 Hz (Cowan and Wilson 1994). The frequency of up states varies in other areas or preparations, including: 1.8 Hz in ferret piriform cortex *in vitro* (Sanchez-Vives et al. 2008), lower frequencies in rat entorhinal cortex *in vitro* varying between 0.17 Hz (Cunningham et al. 2006) and 0.02Hz (Mann et al. 2009), and still lower in cortical slabs (0.002-0.008 Hz) (Timofeev et al. 2000) . This diversity of frequencies imply that down states vary between 0.5 s and over 1 min and thus must respond to the participation of different network mechanisms. In cases where the average duration of the down states lasts tens of seconds, K^+ channel activation is probably not the main mechanism that maintains the complete duration of down states. Afterhyperpolarizations (AHPs) are often observed following up states (Sanchez-Vives and McCormick, 2000) and they increased for higher preceding firing rates (Fig. 8). However, the discharge in an up state is not enough to induce AHPs that would last for as long as a 10 s-down state. We propose that the mechanism determining the duration of down states in these cases is not an AHP but the time it takes for the mechanisms that give rise to a new up state to build up. For example, summation of randomly occurring miniature synaptic potentials is a mechanism proposed for up state initiation in cortical slabs where up states occur at frequencies well below 0.2 Hz, with down states of up to 60 s (Timofeev et al. 2000).

Transitions between up and down states and wave propagation

The transition from down to up state corresponds to the recruitment of the local network. A network that is recruited faster has a steeper slope in the transition and vice versa, and we have shown this here both for the population firing rate and for the accumulation of synaptic potentials while recorded intracellularly. Excitation and inhibition accumulate at a similar rate during the down to up transition in cortical slices (Compte et al. 2009; Shu et al. 2003b). The EPSPs impinging onto cortical neurons in cortical slices may originate in distant excitatory neurons through horizontal connections or in local ones, while IPSPs are originated in local interneurons. Long horizontal connections also have inhibitory interneurons as a target (20%), although in lesser proportion than excitatory target neurons (80%) (McGuire et al. 1991). Therefore, excitatory neurons that are firing during an up state would contribute to the build up of excitatory and inhibitory activity in the distant regions they project to. This initial depolarization still requires the local reverberation of activity in order to generate an up state, which appears to activate local neurons in an stereotypical order (Luczak et al. 2007). The local reverberation necessary for wave propagation is probably the reason why there is a relationship between the speed of wave propagation and the slope of the transition from down to up states (Fig. 5D). Long range connectivity in the cortical model had relevant influence in the speed of wave propagation, decreasing with the length of horizontal connections (Compte et al. 2003). Progressive elimination of network inhibition accelerates the transition from down to up states, synaptic events accumulating faster. Not only distant excitation is then balanced towards excitation, but the local circuit is also not slowed down by inhibitory summation. Still, the progressively faster propagation with the removal of inhibition is nonlinear towards the highly fast propagation of epileptiform activity (Fig. 5C; 6A). The speed of wave propagation approximately doubles with progressive inhibition blockade, but then it leaps towards speeds almost one order of magnitude higher when epileptiform activity appears, as in (Sanchez-Vives and McCormick 2000). Epileptiform bursts should thus not be seen as the last step of a progressive

transformation of up states when inhibition is removed, since every aspect of them are the result of a nonlinear change. Radically different network mechanisms are at play.

The transition from up to down states also increases its rate with the removal of inhibition. The more efficient activation of K^+ channels following a higher firing rate during up states would induce neuronal AHPs (Compte et al. 2003). Since the up state maintenance requires reverberation of activity in the network, this sudden hyperpolarization would stop this process and induce a transition towards the down state. A faster network transition would therefore reflect a more synchronized end of the reverberatory activity, associated to lesser inhibition. A similar mechanism based on K^+ channel recruitment terminates epileptiform bursts in hippocampus (Alger and Nicoll 1980). Even when the mechanisms that determine the down to up and the up to down transitions are totally different, they seem to covary. We have found the same covariation in the transformation of slow oscillations with temperature (Reig et al. 2010). The link between both slopes is the firing rate during up states. A fast upward transition is usually associated to a high frequency rate once the up state occurs, which will normally induce a fast transition towards the next down or silent state.

Sufficient mechanisms: recurrent coupling and adaptation channels

We used a computational network model of the slow oscillation (Compte et al., 2003) and prove that the combination of strong recurrent coupling and activity-dependent hyperpolarizing currents was sufficient to explain the modulations of network activity patterns induced by inhibition manipulations in our experiments. Investigations with the model network showed the same trends in up state firing rate, up state duration, down state duration, down-to-up transition slope and wave propagation speed than experiments upon gradual inhibitory transmission manipulations. At least qualitatively, the control of network activity by inhibition during the slow oscillation *in vitro* can be understood primarily as the interplay of excitation, inhibition and slow adaptation currents. This underscores the importance of adaptation currents in the control of physiological network activity, and suggests its possible compensatory role upon failing inhibitory regulation.

Grants:
Supported by the Spanish Ministry of Science (MICINN) to MVSV and AC. MW was funded by FPI fellowship (MICINN).

Figure captions

Figure 1. Effects of progressive inhibition blockade on slow oscillations.
A: Raw multiunit recording (blue trace), relative firing rate (black trace; see Materials and Methods). Up states were detected on the relative firing rate (red trace). The transformation of spontaneous slow oscillations with bicuculline is shown. From top to bottom: control activity, 0.4 μM, 1.2μM and 3 μM. **B:** Raster plots of the relative firing rate. 100 aligned up states are represented for each bicuculline concentration corresponding to the ones in A. The firing rate is colour coded. **C:** Average relative firing rate for up states during the control and 6 increasingly higher concentrations of bicuculline. The shadow corresponds to the s.e.m. Notice the progressive shortening of up states and increase in firing rate with the removal of inhibition. **D:** Autocorrelograms illustrating the transformation of the emerging activity in control (left) and 1.2 μM bicuculline (right). **E:** Histograms of the relative firing rate values illustrating the bimodality for control (left) and 1.2 μM bicuculline (right). **F:** Shortening of the duration of up states and **G:** increase in relative firing rate during up states with the progressive blockade of inhibition in this particular case.

Figure 2. Transformation of up and down states during the progressive removal of inhibition, population average.
A: Representation of frequency of up/down cycles, **B:** relative firing rate **C:** up states duration and **D:** down state duration for increasingly higher bicuculline concentrations in the bath.

Figure 3. Evolution of transitions between up and down states with the removal of inhibition.
A: A case illustrating the progressive increase of the firing rate slope of down to up state transition for control and 5 increasing concentrations of bicuculline (see colour code). **B:** Average increase in the slope of the upward transition in the population. **C:** Same case as in A illustrating the progressive increase of the slope of firing rate decrease during the transition from up to down state for control and 5 concentrations

of bicuculline (see colour code). **D:** Average increase in the slope of the upward transition in the population. **E:** From top to bottom, three raw traces of the intracellular recordings that here were maintained subthreshold (Vm=-84 mV). From left to right, control up states and increasing blockade of inhibition induced by the local application of 200 μM BMI. This is the intracellular counterpart of the progressive increase in down to up state transition slope (in red) during the progressive removal of inhibition. The slope here represents the accumulation of synaptic potentials building up towards the up state. In blue, the downward transition slope illustrates the termination of up states. The slope was calculated by fitting a line to the membrane potential values during the transition (inset). For all measures $p<0.0001$, R value between 0.83 and 0.98. Note the progressive increase in the upward and downward slope; the values of the slope are displayed.

Figure 4. Appearance of "diplets" during reduced inhibition. A: Spontaneous up and down states. Example of intracellular (top trace) and multiunit recording (bottom trace). **B:** Spontaneous rhythmic activity after local application of bicuculline (100 μM). Note that the up states are transformed in "diplets", or doubled up states. **C:** Twelve minutes after starting the washing out of bicuculline. **D**: Spontaneous activity 30 minutes after washing out bicuculline (Vm=-64mV). **E:** The vertical black lines indicate the times of occurrence of individual "diplets" during steps of progressive inhibition removal in 3 cases. Note that in 2 of them (traces 1 and 3) it was a transitory effect, and by the time that epileptiform activity occurred (discontinuous red lines), "diplets" had already dissapeared. **F:** Raster plots illustrating up states or "diplets" (in red) for the case in panel E3 for different concentrations of bicuculline. Note that "diplets" had hardly appeared at 0.2 μM and their frequency increased at 0.6 μM. At 1 μM up states are shorter and "diplets" were not occurring anymore.

Figure 5. Effects of decreasing inhibition on propagation of up states across the cortical network.

A: Example of the same up states as recorded from two electrodes separated by 840 μm (BMI = 0.2 μM, 71 extracted up states per rasterplot). Up states were aligned at the

599 electrode 2 (below) and the arrival of the up state at electrode 2 is represented above.
600 **B:** Histogram of time lags for different bicuculline concentrations (colour code). Note
601 how the time lags become shorter for higher bicuculline concentrations. **C:** The speed
602 of propagation between two electrodes was calculated (n=5; circles in colour) for
603 increasingly higher concentrations of bicuculline, and before epileptiform activity was
604 reached. The averaged values are represented as empty squares with error bars (s.e.m.).
605 Inset, average increase of the speed of propagation before epileptiform activity was
606 reached. Note that the speed doubled. When epileptiform activity appeared, the speed
607 of propagation increased significantly. **D:** Relationship between the down to up slope of
608 firing rate at electrodes 1 and 2 and the speed of propagation between them. Same
609 example slice as in panels **A** and **B**. Each symbol represents an extracted couple of up
610 states and different colours code for different bicuculline concentrations (see legend
611 inset in panel B).
612
613 **Figure 6. Epileptiform discharge onset at high disinhibition levels.**
614 **Epileptic rating. A**: Top, the relative firing rates sampled by two simultaneous
615 recordings MU1 and MU2 (grey and black respectively), within the period between the
616 change of BMI concentration from 1 to 1.5 μM (t = 0 s) and the onset of epileptiform
617 discharge. Bottom, latencies between the onsets of up states detected in MU1 and MU2.
618 The shorter the latency, the higher the speed of propagation of up states across the
619 slice. The distance between electrode tips was 0,84 mm. **B:** Magnifications of MUA
620 traces in the underlined traces in A for both, MU1 and MU2. At about 460 s is the onset
621 of the epileptiform discharge. The wider events (one in MU1, two in MU2) correspond
622 to discharge patterns as the ones shown in panel D (stage 2). These are not full-blown
623 epileptiform discharges and in the illustrated cases were local and propagated as
624 normal up states. **C:** Raw traces illustrating the multiunit activity recorded by the
625 electrodes MU1 and MU2 during the same recording shown in A and B. The top two
626 traces correspond to the control, pre-bicuculline up states during slow oscillations. In
627 the bottom two traces, the activity right before the full-blown epileptiform discharge (to
628 the right end of trace) is illustrated. It shows the intermixed occurrence of discharges
629 from stages 1 and 2 (in panel D). **D:** Epileptic rating observed during the progressive

630 removal of inhibition. On stage 0, control up states. On stage 1, shortened up states,
631 still of fusiform shape. On stage 2, a different dynamic state, consisting in not full-
632 blown epileptiform discharges. The shape is not fusiform, but triangular. The shape
633 reflects a very fast upward transition and a slow and progressive decay of the discharge.
634 Stage 3 is the full-blown epileptiform discharge.
635
636 **Figure 7. Reducing inhibition in a cortical network model.**
637 Manipulation of inhibition in a computational network model that relies on recurrent
638 coupling and activity-dependent adaptation mechanisms (Compte et al., 2003)
639 produces the same effects on the duration and interval between up states and on mean
640 firing rate as in experiments. **A:** Sample network rastergram in control. **B:** Sample
641 network rastergram after partial inhibition blockade to a remaining 25% of inhibition
642 relative to control (A). **C:** The activity profiles for model neurons aligned at the
643 beginning of the up state show that reducing inhibition (from control to 50% and
644 further to 25% inhibition) increases firing rates in the up state and the interval between
645 successive up states (down state). **D:** Normalized activity profiles for one up state show
646 how inhibition blockade reduces up state duration and increases down-to-up activation
647 slope. **E**: Summary graph of up state duration (measured as time duration for which
648 curves in panel D exceed 10% of maximum value, black trace) and interval of oscillation
649 (measured as interval between maxima in panel C, red trace) for intermediate values of
650 inhibition in the network (100%, 90%, 80%, 70%, 60%, 50%, 40%, 30%, and 25%)
651 shows progressive gradual changes as in experiments. **F:** Membrane potential traces
652 from two neurons (left and right panels) in the cortical network model during slow
653 oscillations. In both examples, control traces are shown on the left column (traces
654 expanded around resting voltage in the bottom panel). On the right column, membrane
655 potential traces in the same neurons after network inhibition was decreased. Notice the
656 shortening of the up states and the increased after-hyperpolarization following the up
657 states.
658
659 **Figure 8. Aftherhyperpolarizations following up states are increased when**
660 **there is lesser inhibition. A:** Intracellular recordings of a neuron in an oscillating

slice in control (left) and during the partial blockade of inhibition with bicuculline (right). The bottom trace is expanded to better see the increased afterhyperpolarization that followed up states when inhibition was partially blocked. **B:** Multiunit recording of network activity in the close vicinity of the intracellular recording shown in A. **C, D:** represent another neuron example equivalent to A, B in a different slice. Vertical scale bar corresponds to 10 mV and horizontal scale bar to 1 s.

References

Aghajanian GK and Rasmussen K. Intracellular studies in the facial nucleus illustrating a simple new method for obtaining viable motoneurons in adult rat brain slices. In: *Synapse*, 1989, p. 331-338.

Alger BE and Nicoll RA. Epileptiform burst afterhyperolarization: calcium-dependent potassium potential in hippocampal CA1 pyramidal cells. *Science* 210: 1122-1124, 1980.

Anderson JS, Carandini M, and Ferster D. Orientation tuning of input conductance, excitation, and inhibition in cat primary visual cortex. *J Neurophysiol* 84: 909-926, 2000.

Belichenko PV, Masliah E, Kleschevnikov AM, Villar AJ, Epstein CJ, Salehi A, and Mobley WC. Synaptic structural abnormalities in the Ts65Dn mouse model of Down Syndrome. *J Comp Neurol* 480: 281-298, 2004.

Borg-Graham LJ, Monier C, and Fregnac Y. Visual input evokes transient and strong shunting inhibition in visual cortical neurons. *Nature* 393: 369-373, 1998.

Brown P, Ridding MC, Werhahn KJ, Rothwell JC, and Marsden CD. Abnormalities of the balance between inhibition and excitation in the motor cortex of patients with cortical myoclonus. *Brain* 119 (Pt 1): 309-317, 1996.

Compte A, Reig R, Descalzo VF, Harvey MA, Puccini GD, and Sanchez-Vives MV. Spontaneous high-frequency (10-80 Hz) oscillations during up states in the cerebral cortex in vitro. *J Neurosci* 28: 13828-13844, 2008.

Compte A, Reig R, and Sanchez-Vives MV. Timing excitation and inhibition in the cortical network. In: *Coherent Behavior in Neuronal Networks*, edited by Josic KR, J.; Matias, M.; Romo, R.: Springer, 2009.

Compte A, Sanchez-Vives MV, McCormick DA, and Wang XJ. Cellular and network mechanisms of slow oscillatory activity (<1 Hz) and wave propagations in a cortical network model. In: *J Neurophysiol*, 2003, p. 2707-2725.

Contreras D, Timofeev I, and Steriade M. Mechanisms of long-lasting hyperpolarizations underlying slow sleep oscillations in cat corticothalamic networks. *J Physiol* 494 (Pt 1): 251-264, 1996.

Cowan RL and Wilson CJ. Spontaneous firing patterns and axonal projections of single corticostriatal neurons in the rat medial agranular cortex. *J Neurophysiol* 71: 17-32, 1994.

Cunningham MO, Pervouchine DD, Racca C, Kopell NJ, Davies CH, Jones RS, Traub RD, and Whittington MA. Neuronal metabolism governs cortical network response state. *Proc Natl Acad Sci U S A* 103: 5597-5601, 2006.

Dani VS, Chang Q, Maffei A, Turrigiano GG, Jaenisch R, and Nelson SB. Reduced cortical activity due to a shift in the balance between excitation and inhibition in a mouse model of Rett syndrome. *Proc Natl Acad Sci U S A* 102: 12560-12565, 2005.

Debarbieux F, Brunton J, and Charpak S. Effect of bicuculline on thalamic activity: a direct blockade of IAHP in reticularis neurons. *J Neurophysiol* 79: 2911-2918, 1998.

Fernandez F, Morishita W, Zuniga E, Nguyen J, Blank M, Malenka RC, and Garner CC. Pharmacotherapy for cognitive impairment in a mouse model of Down syndrome. *Nat Neurosci* 10: 411-413, 2007.

Gutnick MJ, Connors BW, and Prince DA. Mechanisms of neocortical epileptogenesis in vitro. *J Neurophysiol* 48: 1321-1335, 1982.

Haider B, Duque A, Hasenstaub AR, and McCormick DA. Neocortical network activity in vivo is generated through a dynamic balance of excitation and inhibition. *J Neurosci* 26: 4535-4545, 2006.

Hanson JE, Blank M, Valenzuela RA, Garner CC, and Madison DV. The functional nature of synaptic circuitry is altered in area CA3 of the hippocampus in a mouse model of Down's syndrome. *J Physiol* 579: 53-67, 2007.
Hebb DO. *The organization of behavior*: Wiley, New York, 1949.
Holcman D and Tsodyks M. The emergence of Up and Down states in cortical networks. *PLoS Comput Biol* 2: e23, 2006.
Innocenti GM, Manger PR, Masiello I, Colin I, and Tettoni L. Architecture and callosal connections of visual areas 17, 18, 19 and 21 in the ferret (Mustela putorius). *Cereb Cortex* 12: 411-422, 2002.
Khawaled R, Bruening-Wright A, Adelman JP, and Maylie J. Bicuculline block of small-conductance calcium-activated potassium channels. *Pflugers Arch* 438: 314-321, 1999.
Krimer LS and Goldman-Rakic PS. Prefrontal microcircuits: membrane properties and excitatory input of local, medium, and wide arbor interneurons. *J Neurosci* 21: 3788-3796, 2001.
Kumar SS and Buckmaster PS. Hyperexcitability, interneurons, and loss of GABAergic synapses in entorhinal cortex in a model of temporal lobe epilepsy. *J Neurosci* 26: 4613-4623, 2006.
Kurt MA, Kafa MI, Dierssen M, and Davies DC. Deficits of neuronal density in CA1 and synaptic density in the dentate gyrus, CA3 and CA1, in a mouse model of Down syndrome. *Brain Res* 1022: 101-109, 2004.
Lampl I, Reichova I, and Ferster D. Synchronous membrane potential fluctuations in neurons of the cat visual cortex. 22: 361-374, 1999.
Lorente de Nó R. Analysis of the activity of the chains of internuncial neurons. *Journal of Neurophysiology* 1: 207-244, 1938.
Luczak A, Bartho P, Marguet SL, Buzsaki G, and Harris KD. Sequential structure of neocortical spontaneous activity in vivo. *Proc Natl Acad Sci U S A* 104: 347-352, 2007.
Mann EO, Kohl MM, and Paulsen O. Distinct roles of GABA(A) and GABA(B) receptors in balancing and terminating persistent cortical activity. *J Neurosci* 29: 7513-7518, 2009.
Mattia M and Del Giudice P. Population dynamics of interacting spiking neurons. *Phys Rev E* 66: 1-19, 2002.
McGuire BA, Gilbert CD, Rivlin PK, and Wiesel TN. Targets of horizontal connections in macaque primary visual cortex. *J Comp Neurol* 305: 370-392, 1991.
Monier C, Fournier J, and Fregnac Y. In vitro and in vivo measures of evoked excitatory and inhibitory conductance dynamics in sensory cortices. *J Neurosci Methods* 169: 323-365, 2008.
Nowak LG, Azouz R, Sanchez-Vives MV, Gray CM, and McCormick DA. Electrophysiological classes of cat primary visual cortical neurons in vivo as revealed by quantitative analyses. *J Neurophysiol* 89: 1541-1566, 2003.
Okun M and Lampl I. Instantaneous correlation of excitation and inhibition during ongoing and sensory-evoked activities. *Nat Neurosci* 11: 535-537, 2008.
Pare D, Shink E, Gaudreau H, Destexhe A, and Lang EJ. Impact of spontaneous synaptic activity on the resting properties of cat neocortical pyramidal neurons In vivo. *J Neurophysiol* 79: 1450-1460, 1998.
Parga N and Abbott LF. Network model of spontaneous activity exhibiting synchronous transitions between up and down States. *Front Neurosci* 1: 57-66, 2007.
Prince DA and Wilder BJ. Control mechanisms in cortical epileptogenic foci. "Surround" inhibition. *Arch Neurol* 16: 194-202, 1967.

Reig R, Mattia M, Compte A, Belmonte C, and Sanchez-Vives MV. Temperature Modulation of Slow and Fast Cortical Rhythms. *J Neurophysiol* 103: 1253-1261, 2010.
Rubenstein JL and Merzenich MM. Model of autism: increased ratio of excitation/inhibition in key neural systems. *Genes Brain Behav* 2: 255-267, 2003.
Rudolph M, Pospischil M, Timofeev I, and Destexhe A. Inhibition determines membrane potential dynamics and controls action potential generation in awake and sleeping cat cortex. *J Neurosci* 27: 5280-5290, 2007.
Sanchez-Vives MV, Descalzo VF, Reig R, Figueroa NA, Compte A, and Gallego R. Rhythmic spontaneous activity in the piriform cortex. *Cereb Cortex* 18: 1179-1192, 2008.
Sanchez-Vives MV and McCormick DA. Cellular and network mechanisms of rhythmic recurrent activity in neocortex. In: *Nat Neurosci*, 2000, p. 1027-1034.
Shadlen MN and Newsome WT. The variable discharge of cortical neurons: implications for connectivity, computation, and information coding. *J Neurosci* 18: 3870-3896, 1998.
Shu Y, Hasenstaub A, Badoual M, Bal T, and McCormick DA. Barrages of synaptic activity control the gain and sensitivity of cortical neurons. *J Neurosci* 23: 10388-10401, 2003a.
Shu Y, Hasenstaub A, and McCormick DA. Turning on and off recurrent balanced cortical activity. *Nature* 423: 288-293, 2003b.
Stark E and Abeles M. Predicting movement from multiunit activity. *J Neurosci* 27: 8387-8394, 2007.
Steriade M, Amzica F, Neckelmann D, and Timofeev I. Spike-wave complexes and fast components of cortically generated seizures. II. Extra- and intracellular patterns. *J Neurophysiol* 80: 1456-1479, 1998.
Steriade M and Contreras D. Relations between cortical and thalamic cellular events during transition from sleep patterns to paroxysmal activity. *J Neurosci* 15: 623-642, 1995.
Steriade M, Nunez A, and Amzica F. A novel slow (< 1 Hz) oscillation of neocortical neurons in vivo: depolarizing and hyperpolarizing components. *J Neurosci* 13: 3252-3265, 1993.
Steriade M, Timofeev I, and Grenier F. Natural waking and sleep states: a view from inside neocortical neurons. *J Neurophysiol* 85: 1969-1985, 2001.
Stern EA, Kincaid AE, and Wilson CJ. Spontaneous subthreshold membrane potential fluctuations and action potential variability of rat corticostriatal and striatal neurons in vivo. *J Neurophysiol* 77: 1697-1715, 1997.
Timofeev I, Grenier F, Bazhenov M, Sejnowski TJ, and Steriade M. Origin of slow cortical oscillations in deafferented cortical slabs. *Cereb Cortex* 10: 1185-1199, 2000.
Timofeev I, Grenier F, and Steriade M. The role of chloride-dependent inhibition and the activity of fast-spiking neurons during cortical spike-wave electrographic seizures. *Neuroscience* 114: 1115-1132, 2002.
Wang XJ. Synaptic basis of cortical persistent activity: the importance of NMDA receptors to working memory. In: *J Neurosci*, 1999, p. 9587-9603.
Wang XJ and Buzsaki G. Gamma oscillation by synaptic inhibition in a hippocampal interneuronal network model. In: *J Neurosci*, 1996, p. 6402-6413.
Wehr M and Zador AM. Balanced inhibition underlies tuning and sharpens spike timing in auditory cortex. *Nature* 426: 442-446, 2003.

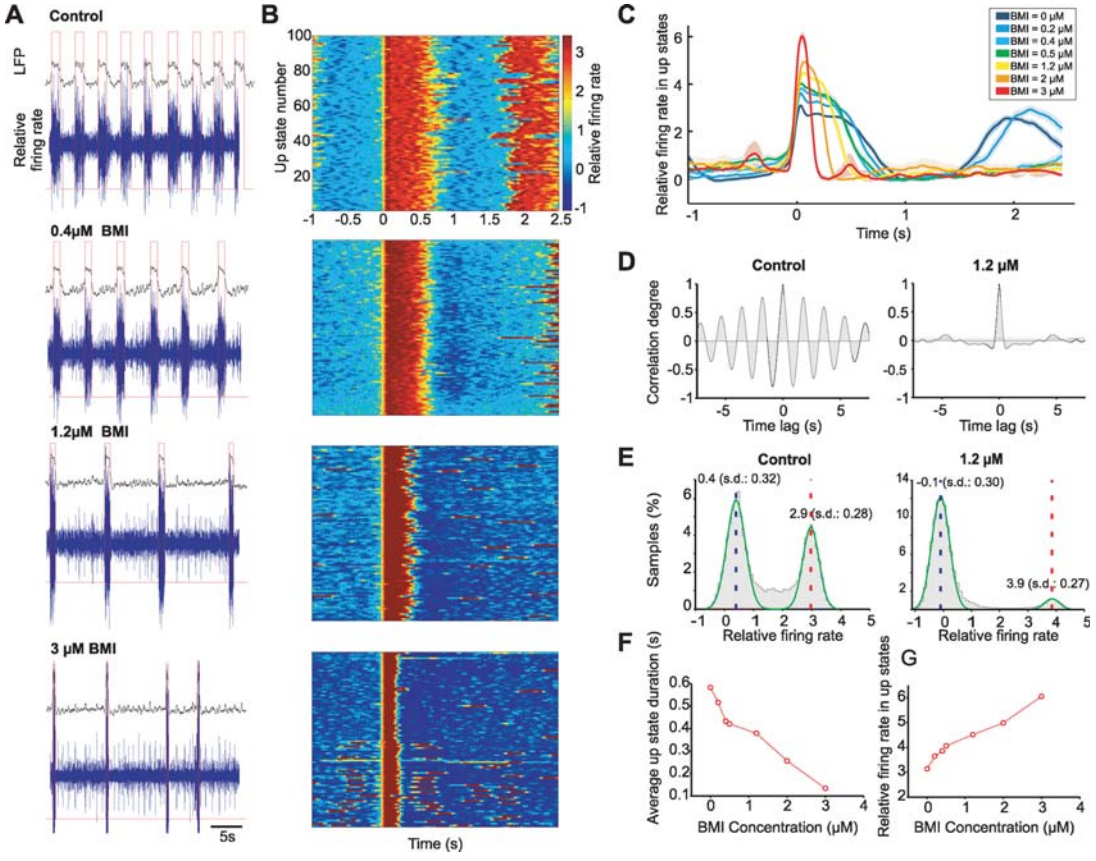
A
Control
LFP
Relative firing rate
0.4μM BMI
1.2μM BMI
3 μM BMI
5s
B
Up state number
Relative firing rate
Time (s)
C
BMI = 0 μM
BMI = 0.2 μM
BMI = 0.4 μM
BMI = 0.5 μM
BMI = 1.2 μM
BMI = 2 μM
BMI = 3 μM
Relative firing rate in up states
Time (s)
D
Control
1.2 μM
Correlation degree
Time lag (s)
E
Control
1.2 μM
Samples (%)
0.4 (s.d.: 0.32)
2.9 (s.d.: 0.28)
-0.1 (s.d.: 0.30)
3.9 (s.d.: 0.27)
Relative firing rate
F
Average up state duration (s)
BMI Concentration (μM)
G
Relative firing rate in up states
BMI Concentration (μM)

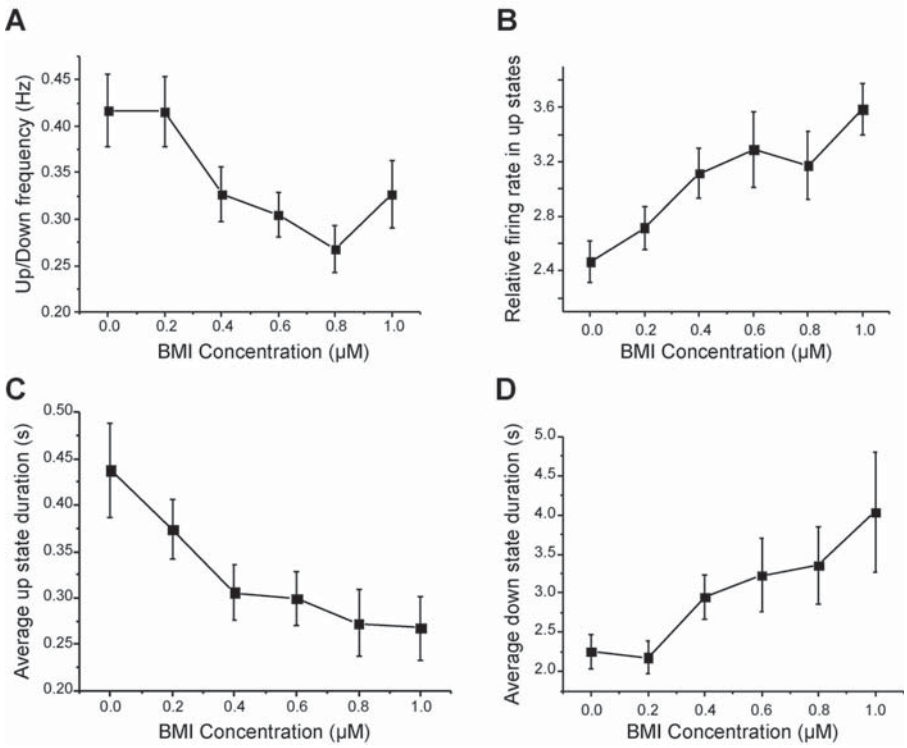
A
Up/Down frequency (Hz)
0.45
0.40
0.35
0.30
0.25
0.20
0.0
0.2
0.4
0.6
0.8
1.0
BMI Concentration (μM)
B
Relative firing rate in up states
3.6
3.2
2.8
2.4
0.0
0.2
0.4
0.6
0.8
1.0
BMI Concentration (μM)
C
Average up state duration (s)
0.50
0.45
0.40
0.35
0.30
0.25
0.20
0.0
0.2
0.4
0.6
0.8
1.0
BMI Concentration (μM)
D
Average down state duration (s)
5.0
4.5
4.0
3.5
3.0
2.5
2.0
0.0
0.2
0.4
0.6
0.8
1.0
BMI Concentration (μM)

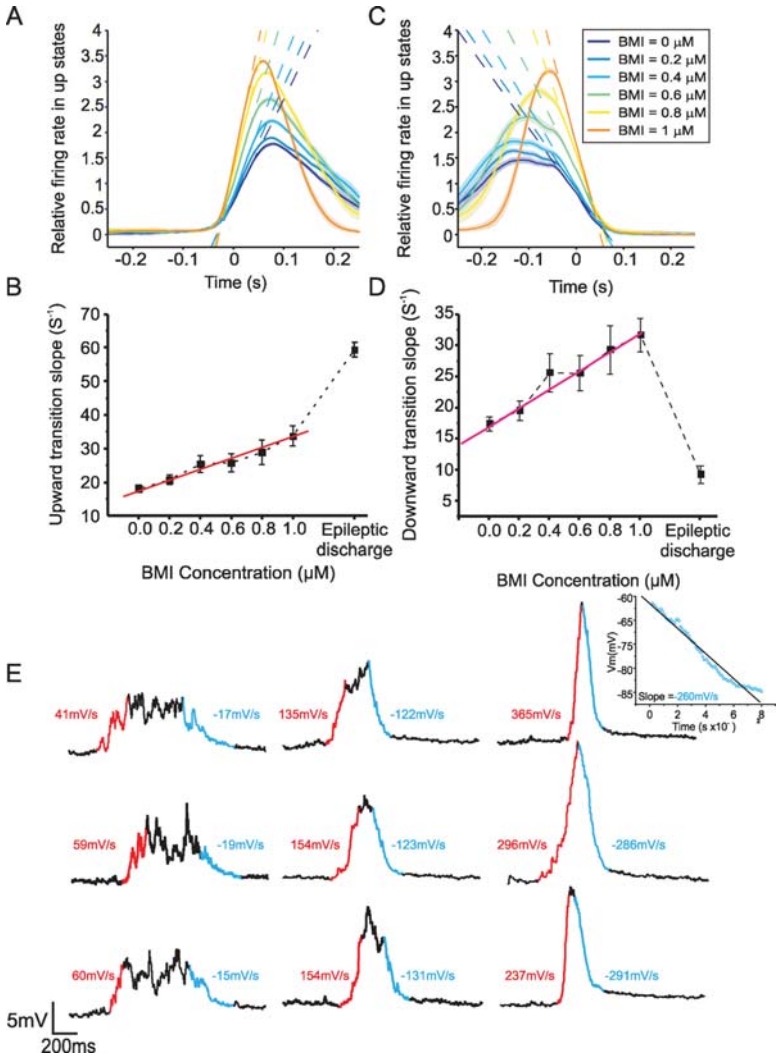
A
Relative firing rate in up states
Time (s)
C
BMI = 0 μM
BMI = 0.2 μM
BMI = 0.4 μM
BMI = 0.6 μM
BMI = 0.8 μM
BMI = 1 μM
B
Upward transition slope (S⁻¹)
Epileptic discharge
BMI Concentration (μM)
D
Downward transition slope (S⁻¹)
E
41mV/s
-17mV/s
135mV/s
-122mV/s
365mV/s
Vm(mV)
Slope = -260mV/s
59mV/s
-19mV/s
154mV/s
-123mV/s
296mV/s
-286mV/s
60mV/s
-15mV/s
154mV/s
-131mV/s
237mV/s
-291mV/s
5mV
200ms

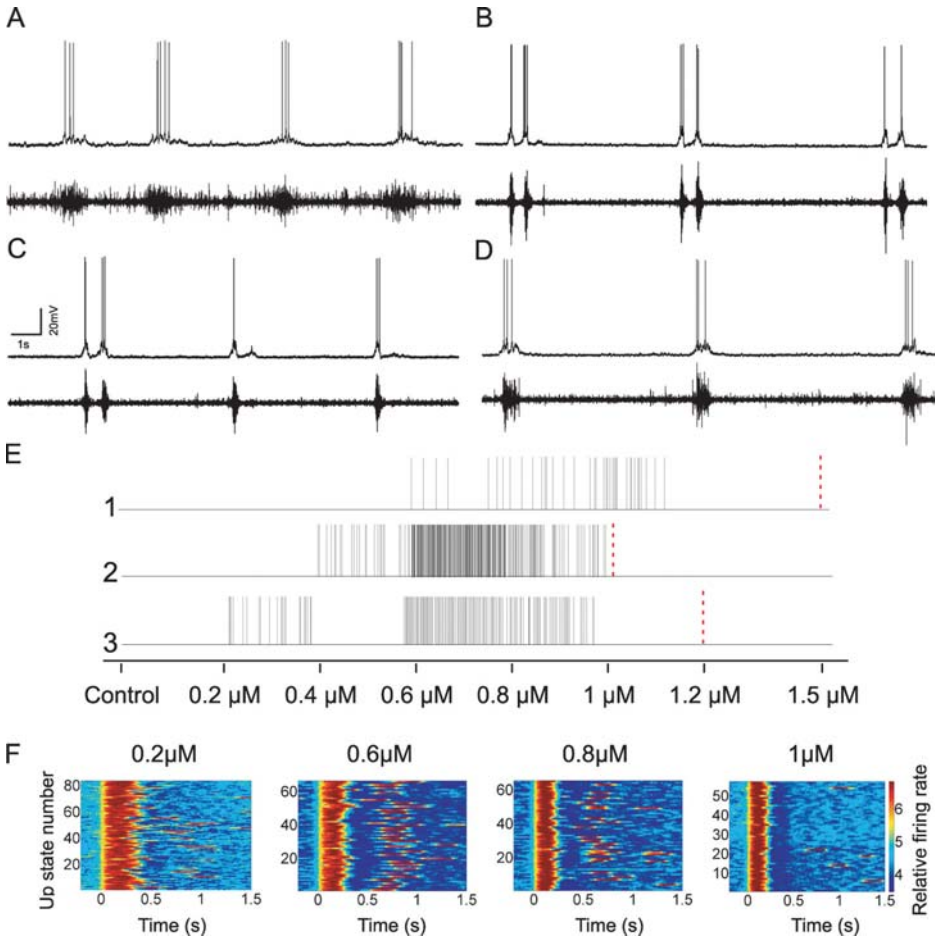
A
B
C
D
20mV
1s
E
1
2
3
Control
0.2 μM
0.4 μM
0.6 μM
0.8 μM
1 μM
1.2 μM
1.5 μM
F
0.2μM
0.6μM
0.8μM
1μM
Up state number
Time (s)
Relative firing rate

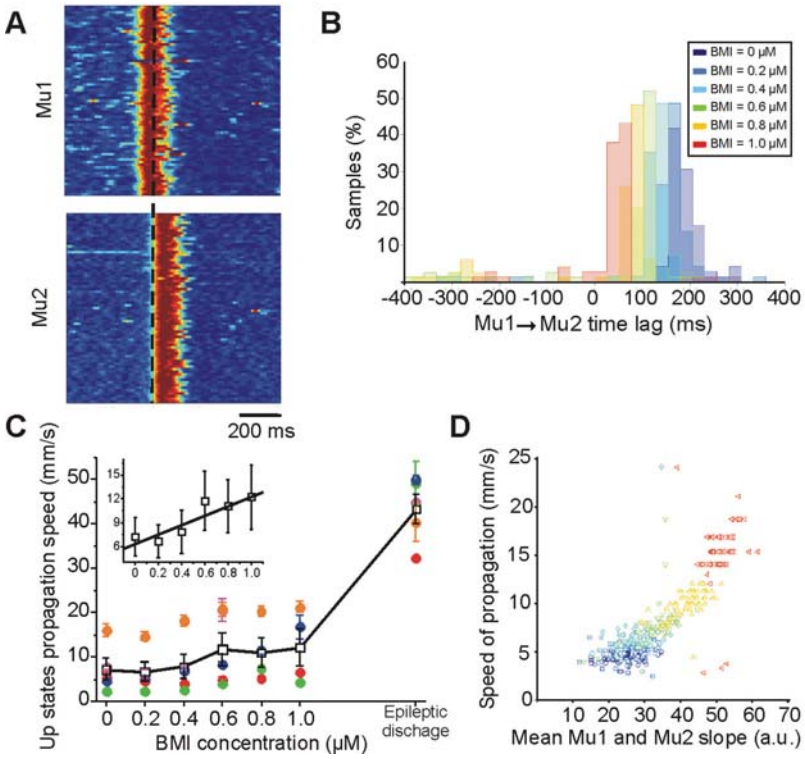
A
Mu1
Mu2
200 ms
B
BMI = 0 µM
BMI = 0.2 µM
BMI = 0.4 µM
BMI = 0.6 µM
BMI = 0.8 µM
BMI = 1.0 µM
Samples (%)
Mu1→Mu2 time lag (ms)
C
Up states propagation speed (mm/s)
BMI concentration (µM)
Epileptic dischage
D
Speed of propagation (mm/s)
Mean Mu1 and Mu2 slope (a.u.)

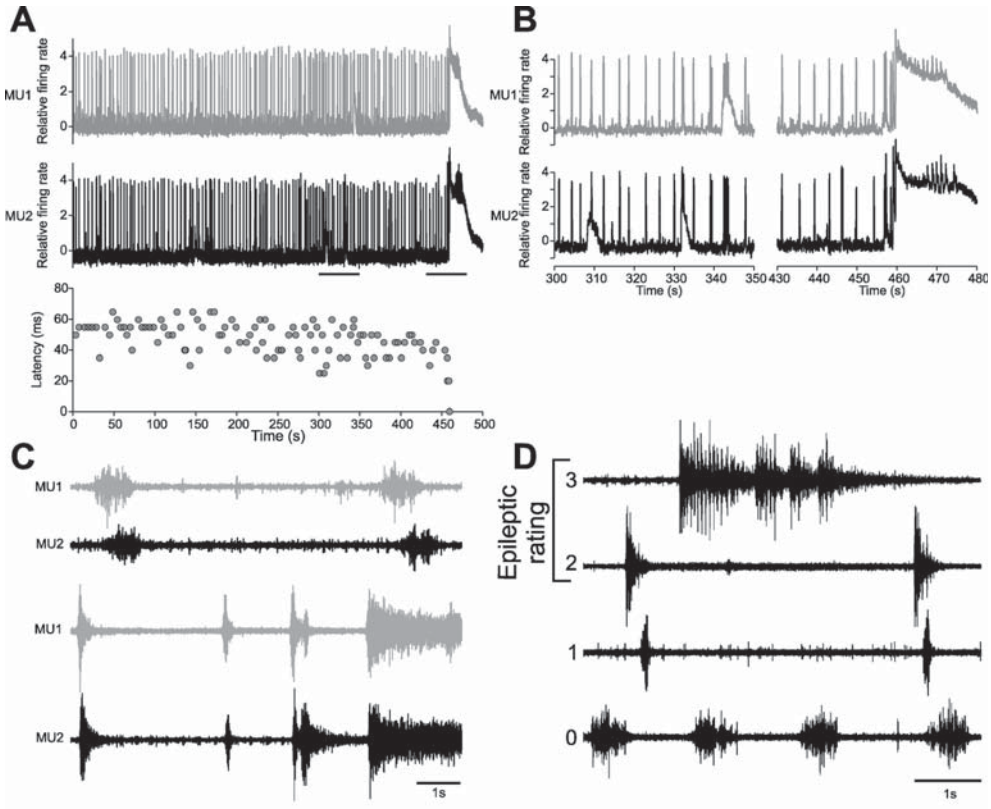
A
MU1
Relative firing rate
MU2
Relative firing rate
Latency (ms)
Time (s)
B
MU1
Relative firing rate
MU2
Relative firing rate
Time (s)
Time (s)
C
MU1
MU2
MU1
MU2
1s
D
Epileptic rating
3
2
1
0
1s

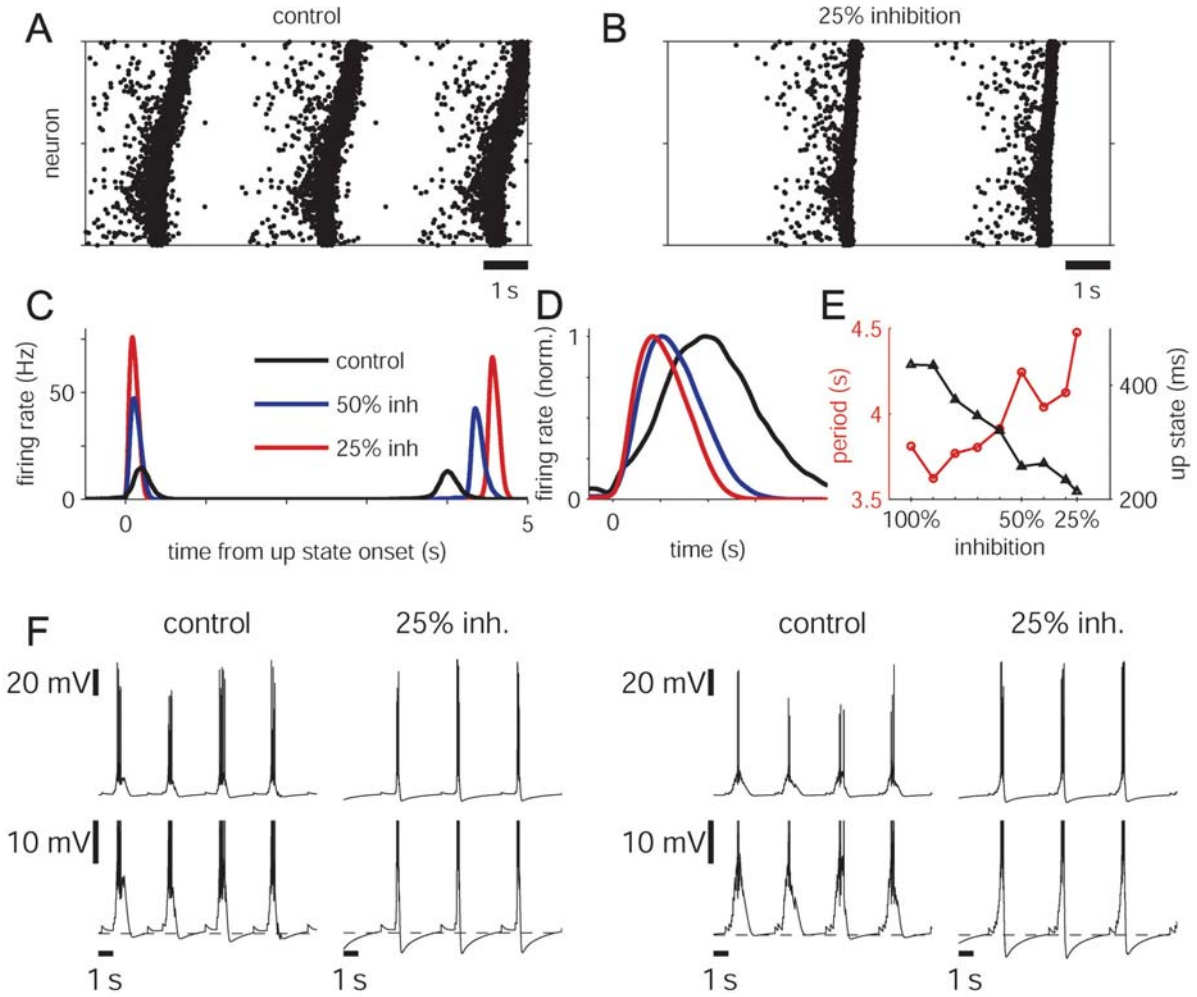
A
control
neuron
1 s
B
25% inhibition
1 s
C
firing rate (Hz)
50
0
control
50% inh
25% inh
0
5
time from up state onset (s)
D
firing rate (norm.)
1
0
0
time (s)
E
4.5
4
3.5
period (s)
400
200
up state (ms)
100%
50%
25%
inhibition
F
control
25% inh.
20 mV
10 mV
1 s
1 s
control
25% inh.
20 mV
10 mV
1 s
1 s

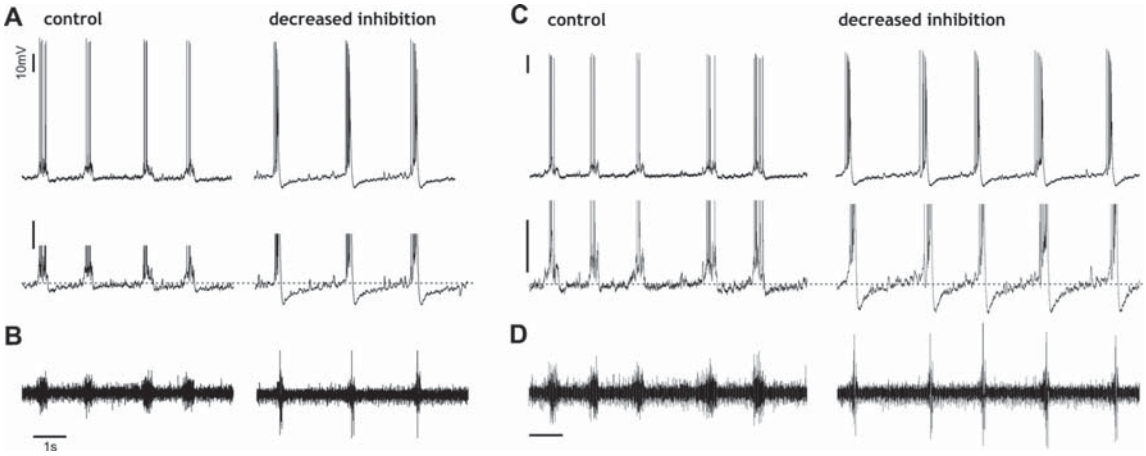
A
control
decreased inhibition
10mV
B
1s
C
control
decreased inhibition
D